Modeled rapid adjustments in diurnal temperature range response to CO_2 and solar forcings

Lawrence S. Jackson[1] and Piers M. Forster[1]

Received 15 May 2012; revised 28 January 2013; accepted 31 January 2013; published 14 March 2013.

[1] We used the National Center for Atmospheric Research single column climate model to determine if rapid adjustments to surface heat fluxes contribute to a change in skin surface or surface air diurnal temperature range (DTR) under $2 \times CO_2$ and -2% solar forcings. An ensemble of model runs was employed with locations selected to represent a range of different climatic conditions and with forcing implemented hourly throughout the diurnal cycle. The change in skin surface DTR and surface energy fluxes during the 3 days after forcing were used to quantify the rapid adjustment response and temperature related feedback. Averaged over all locations, skin surface DTR reduced by 0.01°C after CO_2 forcing and included a rapid adjustment to skin surface DTR of −0.12°C. Skin surface DTR reduced by 0.17°C after solar forcing and included a rapid adjustment of −0.01°C. The rapid adjustments in skin surface DTR were associated with rapid adjustments in surface sensible and latent heat fluxes necessary to balance the energy budget immediately after forcing. We find that the sensitivity of skin surface DTR to mean temperature related feedback is the same for CO_2 and solar forcings when skin surface DTR rapid adjustments are allowed for. Rapid adjustments played a key role in the geographic variation of the skin surface DTR response to forcing. Our results suggest that diurnal variations in trends of downwelling longwave radiation and rapid reductions in DTR associated with CO_2 forcing potentially contributed to the observed global trend in surface air DTR.

Citation: Jackson, L. S., and P. M. Forster (2013), Modeled rapid adjustments in diurnal temperature range response to CO_2 and solar forcings, *J. Geophys. Res. Atmos.*, *118*, 2229–2240, doi:10.1002/jgrd.50243.

1. Introduction

[2] Annual mean diurnal temperature range (DTR) for surface air over land decreased during the period 1950–2004 by 0.07°C per decade due to a greater rate of increase in daily minimum temperatures (0.20°C per decade) compared to daily maximum temperatures (0.14°C per decade) [*Vose et al*., 2005; *Trenberth et al*., 2007]. Detrended variations in global DTR are weakly correlated with detrended variations in global mean temperature [*Braganza et al*., 2004]. The forcings and feedbacks responsible for the trend in DTR may, therefore, differ from those for global mean temperature. Indeed, simulated trends in surface shortwave (SW) radiation, surface downwelling longwave (LW) radiation, and DTR for surface air over land for the period 1950–1999 [*Zhou et al*., 2010] showed changes in DTR were correlated with the changes in net SW radiation while changes in LW radiation were correlated with the warming of annual mean temperature.

[3] Investigating the response of DTR to an increase in atmospheric carbon dioxide (CO_2) has generally been approached by modeling a step change in CO_2 concentration and calculating the response in DTR and surface energy fluxes some time after the forcing, typically when climate equilibrium was achieved. Without feedback, an increase in atmospheric CO_2 causes a relatively small reduction in DTR [*Hansen et al*., 1995]. The CO_2-driven change in DTR is mainly attributed to the reduction in surface SW radiation from increased atmospheric absorption of near-infrared radiation by CO_2 that limits the warming of maximum temperatures [*Cao et al*., 1992; *Stenchikov and Robuck*, 1995; *Watterson*, 1997]. In contrast, the increase in surface downwelling LW radiation warms maximum and minimum temperatures broadly equally [*Stenchikov and Robuck*, 1995]. Increased surface sensible heat fluxes (SHF) and latent heat fluxes (LHF) also act to reduce surface air DTR through transferring heat away from the surface more effectively in daytime, mitigating the daytime increase in temperature [*Cao et al*., 1992].

[4] Feedbacks associated with a CO_2-induced warmer, wetter climate have been identified as more influential in reducing DTR [e.g., *Stenchikov and Robuck*, 1995]. The impact of water vapor feedback on DTR, with enhanced near-infrared absorption of solar radiation in the atmosphere, was found to be approximately seven times stronger than the reduction in DTR caused by CO_2 alone [*Cao et al*., 1992; *Watterson*, 1997]. The observed reduction in DTR in synoptic weather reports during the period 1980–1991 over a wide land area was linked to observed increases in daytime cloud

[1]School of Earth and Environment, The University of Leeds, UK.

Corresponding author: L. S. Jackson, School of Earth and Environment, The University of Leeds, Leeds, LS2 9JT, UK. (l.s.jackson@leeds.ac.uk)

2169-897X/13/10.1002/jgrd.50243

cover that reduced maximum temperatures [*Dai et al*., 1999]. *Stone and Weaver* [2003] found that, in addition to the influence of the radiative effects of clouds on maximum temperatures, the heat capacity of soil, which is very sensitive to moisture content, exerts a controlling influence on minimum temperatures. Surface shortwave radiation is sensitive to changes in cloud cover and aerosol concentrations, factors that have also been linked to trends in surface air DTR. Dimming and subsequent brightening of surface shortwave radiation has been correlated with global trends in surface air DTR [*Wild et al*., 2007]. These studies point to complex causes of surface air DTR trends driven by diurnal variations in multiple forcings and associated feedback. They present a challenge to climate models, which in a 12-member climate model ensemble simulated only 22% of the global DTR trend for 1950–1999 [*Zhou et al*., 2010].

[5] Surface energy fluxes, clouds and precipitation, in climate model simulations of CO_2 forcing, have been found to undergo rapid adjustment in the first five days following forcing [*Dong et al*., 2009]. In contrast to longer-term feedback, the rapid adjustments are not linearly related to the change in mean temperature. The difference in radiative forcing between the top of atmosphere and the surface, combined with the small heat capacity of the atmosphere, can drive rapid responses in surface heat fluxes and the hydrological cycle [*Gregory* and *Webb*, 2008]. For example, *Andrews et al*. [2009] found the surface LHF reduced rapidly following CO_2 forcing, balancing out the weaker radiative component of the forcing at the surface against stronger tropospheric energy flux changes. The physical response of vegetation to CO_2 can also drive rapid adjustments in the hydrological cycle. Using climate model simulations, *Doutriaux-Boucher et al*. [2009] demonstrated that reduced stomatal conductance in response to CO_2 forcing can cause a reduction in low level cloud cover leading to a rapid increase in surface net SW radiation.

[6] In this study, we use an ensemble of single column climate model runs with the forcing applied at hourly intervals over the diurnal cycle, to simulate the response of skin surface and surface air DTR and surface energy fluxes to CO_2 and solar forcings. We isolate forcings and rapid adjustments of surface heat fluxes from temperature related feedback and investigate whether CO_2 and/or solar forcing can induce a rapid adjustment in DTR itself. We examine changes in temperature and surface energy fluxes during the 3 day period immediately after forcing. Although our chosen climate model will have deficiencies in its simulation of the diurnal cycle and our results will be sensitive to uncertainties in the model parameters, our analysis of the change in DTR between forcing, feedback and rapid adjustment components can perhaps guide model development. Our analysis can also provide insight into, although not an explanation for, observed surface air DTR trends.

2. Experimental Setup

2.1. Data, Model, and Experimental Setup

[7] The National Center for Atmospheric Research (NCAR) single column model was used (SCCM) [*Hack et al*., 2004]. It is a one-dimensional time-dependent model. Governing equations for thermodynamics and momentum are coupled through parameterized physics and depend on specified horizontal flux divergences and specified large-scale vertical motion. The atmospheric component of SCCM [*Collins et al*., 2004] has 26 vertical levels, a T42 horizontal spectral resolution and a 128 × 64 global longitude/latitude grid from which the single columns can be selected. Physics parameterizations are the same as used by the NCAR CAM3 atmospheric model. The atmospheric column is coupled to a single column from the NCAR land model CLM2 that has 10 vertical levels for heat and moisture fluxes [*Oleson et al*., 2004]. The exchange of heat, moisture and momentum between the atmosphere and surface uses a bulk exchange formulation. Atmospheric inputs to the land component of SCCM include SW radiation (split between direct and diffuse radiation and between visible and near-infrared parts of the spectrum) and downwelling LW radiation in addition to measures of the thermodynamic state of the atmosphere, wind and precipitation. Land inputs to the atmospheric column include surface SHF and LHF, water vapor flux, emitted LW radiation, surface albedo and momentum fluxes. Although the CLM2 land model provides only a simplified treatment of terrestrial processes, it was specifically designed for coupling with an atmospheric column and simulating land-atmosphere interactions. CLM2 includes subgrid-scale representations of hydrological and thermal properties for different soils and vegetation types.

[8] Two changes were made to the standard version of the model. First, changes were made to permit the atmospheric CO_2 concentration and total solar irradiance to be changed at the end of a spin-up period and at a user specified time in the diurnal cycle. Second, the model was altered so that perturbations of initial conditions for atmospheric temperature and humidity were identical for each pair of forcing and control runs. The model was configured with 20 min time steps and the parameterization of radiation was calculated hourly.

[9] Horizontal boundary fluxes in and out of the atmospheric column were specified as zero for large-scale temperature and moisture advection. Large-scale vertical motion was also specified as zero. The model setup retains, however, parameterizations for cloud processes, convection (with deep convection treated separately from shallow and mid-level convection), free atmosphere turbulent diffusion and atmospheric boundary level processes for the vertical transport of heat and moisture within a single column during the diurnal cycle. The SCCM model was run at 18 locations representing a variety of land surface and climatic conditions (Figure 1a). The runs commenced on an arbitrary 1 September with initial conditions from a CAM3 generated climatology including horizontal wind profiles fixed at CAM generated climatological values. The model spin-up period was between 5 and 5.5 days, the time taken by the model to achieve stability in meteorology and surface energy fluxes. It varied for individual simulations so that the specific time step of forcing coincided precisely with a full refreshing of solar radiation parameters within the SCCM model.

[10] The CO_2 and solar forcings were applied in separate simulations at the end of the spin-up period. The CO_2 forcing involved a doubling of atmospheric CO_2 concentration from 355 to 710 ppmv, the solar forcing was a 2% reduction in total solar irradiance from 1367 Wm^{-2} to 1340 Wm^{-2}. Temperature and surface energy flux changes were extracted for the first 3 days after forcing.

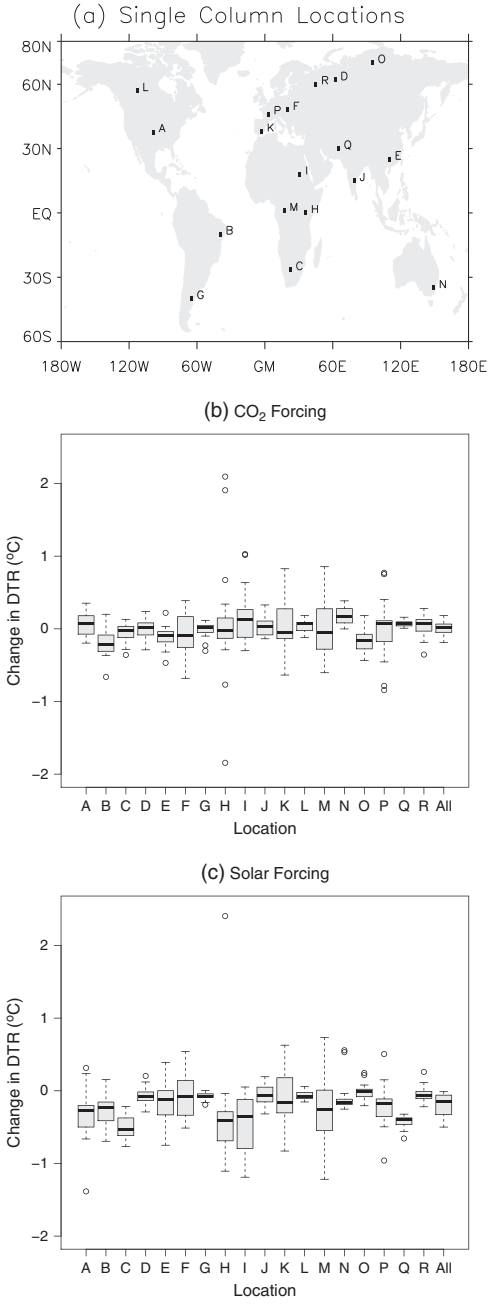

Figure 1. (a) Longitude and latitude for the 18 single column locations labeled "A" to "R". The change in skin surface DTR for ensemble simulations at each location, averaged over the 3 days after (b) CO_2 forcing and (c) solar forcing. The top and bottom of the boxes show the 75th and 25th percentiles; the bold line within each box the median; the dashed line the range of the data and open circles show the extreme data points. "All" represents the distribution of the mean change in skin surface DTR at each location.

[11] The experimental design was inspired, in part, by the approach of *Doutriaux-Boucher et al*. [2009]: they wanted to avoid distortion of CO_2 induced stomatal closure on radiative forcing by the seasonal cycle so ran an ensemble member for each month to determine the seasonal cycle of rapid adjustment. Likewise, we applied the CO_2 and solar forcings each hour of the day in an ensemble of 24 runs at each location. This enabled the change in the complete diurnal cycle of temperature and surface energy fluxes to be determined immediately after the change in forcing. Each ensemble of 24 runs was replicated 20 times in each location by perturbation of initial values for temperature and specific humidity. Climatological values for temperature and specific humidity in each of the 26 atmospheric levels were perturbed separately by random adjustments from a uniform distribution over the range $\pm 0.9°C$ and $\pm 6\%$, respectively. No adjustments were made for vertical auto- or cross-correlation. Identical perturbations were applied to each pair of forcing and control runs.

[12] There were a total of $3 \times 24 \times 20 \times 18$ simulation runs. The response to the forcing was determined from the difference between each pair of forcing and control runs. The 24 runs, with forcing applied at each hour in the day, were used to determine the changes in daily maximum and minimum temperatures giving a total of 20×18 results for the change in DTR. Outliers in the 20 replicates for each location were identified as data points more than 1.5 times the interquartile range from the 25th or the 75th percentile values. The outliers, probably a result of inconsistencies in initial conditions for the atmospheric column, were discarded leaving a total of 349 simulations spread over the 18 locations for CO_2 forcing and 330 simulations for solar forcing.

2.2. Method for Analysis of Results

[13] Preliminary analysis of changes in temperature and surface energy fluxes due to CO_2 and solar forcings showed them to be highly interconnected, which would obscure the physical interpretation of results. The changes in temperature and energy fluxes at each time step after forcing were correlated and affected by interactions between the energy fluxes and the influence of the surface state on the boundary layer response. Trends through time after forcing also exhibited strong correlations and interactions. Linear regression of the change in DTR against changes in surface energy fluxes suffered from multicollinearity, which ridge regression was unsuccessful in addressing.

[14] Changes in surface energy fluxes at the time steps of maximum and minimum temperature, while they do not describe the full evolution of energy fluxes and temperature contributing to the skin surface DTR, provide a means of analyzing the change in skin surface DTR through its decomposition into components linked to changes in individual surface energy fluxes. Assuming the surface energy fluxes are in equilibrium at the time of maximum and minimum temperatures, the net surface energy flux is zero:

$$\mathrm{nSW_x + LWd_x\text{-}LWu_x\text{-}SHF_x\text{-}LHF_x - GHF_x} = 0 \quad (1)$$

$$\mathrm{nSW_n + LWd_n\text{-}LWu_n\text{-}SHF_n\text{-}LHF_n - GHF_n} = 0 \quad (2)$$

where nSW is the net SW radiation; LWd the downwelling LW radiation; LWu the surface emission of LW radiation; SHF, LHF, and GHF the surface sensible, latent, and ground heat fluxes, respectively; and subscripts "x" and "n" represent values at the times of daily maximum and minimum skin surface temperature, respectively. Results from control runs were subtracted from forcing runs at the times of daily maximum and minimum skin surface temperatures to give:

$$\Delta nSW_x + \Delta LWd_x - \Delta LWu_x - \Delta SHF_x - \Delta LHF_x - \Delta GHF_x = 0 \quad (3)$$

$$\Delta nSW_n + \Delta LWd_n - \Delta LWu_n - \Delta SHF_n - \Delta LHF_n - \Delta GHF_n = 0 \quad (4)$$

where "Δ" represents the difference between the forcing and control runs. Approximating surface LW radiation emissions using the Stefan-Boltzmann law with an emissivity of 0.96 (the SCCM assumed emissivity for the ground), the change in surface emission of LW radiation is proportional to the change in skin surface temperature

$$\Delta LWu_x = 0.96 \times 4\sigma T_x^3 \Delta T_x \quad (5)$$

$$\Delta LWu_n = 0.96 \times 4\sigma T_n^3 \Delta T_n \quad (6)$$

where σ is the Stefan-Boltzmann constant, T_x the maximum skin surface temperature and T_n the minimum skin surface temperature. The $4\sigma T_x^3$ term was determined from (5) because ΔLWu_x and ΔT_x were known from the difference between the forcing and control runs. The $4\sigma T_n^3$ term was calculated similarly using (6). Replacing ΔLWu_x and ΔLWu_n in (3) and (4), then rearranging to isolate the change in maximum and minimum temperatures gives

$$\Delta T_x = (\Delta nSW_x + \Delta LWd_x - \Delta SHF_x - \Delta LHF_x - \Delta GHF_x)/3.84\sigma T_x^3 \quad (7)$$

$$\Delta T_n = (\Delta nSW_n + \Delta LWd_n - \Delta SHF_n - \Delta LHF_n - \Delta GHF_n)/3.84\sigma T_n^3 \quad (8)$$

[15] Subtracting (8) from (7) gives

$$\Delta DTR = (\Delta nSW_x + \Delta LWd_x - \Delta SHF_x - \Delta LHF_x - \Delta GHF_x)/3.84\sigma T_x^3 - (\Delta nSW_n + \Delta LWd_n - \Delta SHF_n - \Delta LHF_n - \Delta GHF_n)/3.84\sigma T_n^3 \quad (9)$$

[16] Linear regression was used to split the responses of skin surface DTR and surface energy fluxes to CO_2 and solar forcings into three components: an intercept term used to estimate the rapid adjustment during the 3 days after forcing; a feedback term proportional to the change in mean temperature; and a residual term. The skin surface DTR and surface energy flux responses were analyzed separately for each location using the ensemble mean of simulations produced by perturbation of initial conditions. All regressions were based on ensemble mean data for each time step. A period of 3 days after forcing was used for the regression calculations, consistent with the 2–3 day response time for rapid adjustments over land found by *Dong et al*. [2009]. The mean change in maximum and minimum skin surface temperatures was used as the regression explanatory variable. Different dependent variables were used. First, we used skin surface DTR with results shown in Table 1. Second, we used the mean of the change in surface energy fluxes at the times of maximum and minimum temperatures, hereinafter referred to as the mean change. Finally, we used the difference between the change in surface energy fluxes at the times of maximum temperature and minimum temperature, hereinafter referred to as diurnal asymmetry (adopted from *Stenchikov* and *Robock* [1995]). The ensemble mean changes in surface energy fluxes for each location are shown in Figure 2 (CO_2 forcing) and Figure 4 (solar forcing). The intercept terms from surface energy flux regressions (used to diagnose the rapid adjustments and the direct effects of forcing) are shown in Figure 3 (CO_2 forcing) and Figure 5 (solar forcing) with more detailed results in Tables 2 and 3. The slope terms from surface energy flux regressions (used to diagnose the temperature related feedback) are listed in Tables 2 and 3.

[17] We have adopted a sign convention for surface fluxes consistent with equations (1) to (9). Positive values for net SW and LW radiation represent downward fluxes from the atmosphere to the surface. Positive values for SHF and LHF represent upward fluxes from the surface to the atmosphere. Diurnal asymmetry was calculated as the change in flux at the time of maximum temperature less the change at the time of minimum temperature so that positive values represent either a greater increase, or a

Table 1. Regression of Change in DTR Against the Mean Change in Maximum and Minimum Temperatures[a]

Location	CO_2 Forcing			Solar Forcing		
	R^2	Intercept (°C)	Slope (°C/°C)	R^2	Intercept (°C)	Slope (°C/°C)
A	0.64	**−0.19 ± 0.01**	**1.34 ± 0.07**	0.49	0.02 ±0.02	**1.21 ± 0.08**
B	0.73	**−0.40 ± 0.01**	**1.69 ± 0.07**	0.84	**0.06 ± 0.01**	**1.67 ± 0.05**
C	0.44	**−0.32 ± 0.02**	**1.16 ± 0.09**	0.61	**−0.06 ± 0.02**	**1.55 ± 0.08**
D	0.00	**−0.01 ± 0.00**	0.04 ± 0.05	0.01	**−0.06 ± 0.01**	0.13 ± 0.12
E	0.45	**−0.15 ± 0.01**	**1.27 ± 0.10**	0.34	0.00 ± 0.02	**1.24 ± 0.11**
F	0.75	**−0.25 ± 0.01**	**1.83 ± 0.07**	0.56	**0.02 ± 0.01**	**1.45 ± 0.08**
G	0.75	**−0.08 ± 0.00**	**1.43 ± 0.06**	0.70	0.00 ± 0.00	**1.19 ± 0.05**
H	0.08	−0.03 ± 0.03	**0.61 ± 0.14**	0.31	**−0.04 ± 0.02**	**0.81 ± 0.08**
I	0.72	**−0.16 ± 0.02**	**1.62 ± 0.07**	0.84	0.01 ± 0.02	**2.11 ± 0.06**
J	0.36	**−0.05 ± 0.01**	**1.00 ± 0.09**	0.41	0.01 ± 0.01	**1.07 ± 0.09**
K	0.14	**−0.12 ± 0.02**	**0.78 ± 0.14**	0.02	**−0.24 ± 0.02**	**−0.27 ± 0.12**
L	0.26	0.00 ± 0.00	**0.42 ± 0.05**	0.35	−0.01 ± 0.01	**1.00 ± 0.09**
M	0.61	**−0.08 ± 0.01**	**1.69 ± 0.09**	0.78	**0.14 ± 0.02**	**2.71 ± 0.10**
N	0.80	**−0.10 ± 0.01**	**1.49 ± 0.05**	0.72	**0.04 ± 0.01**	**1.97 ± 0.08**
O	0.00	**−0.07 ± 0.01**	0.08 ± 0.13	0.05	**−0.04 ± 0.01**	**−0.41 ± 0.12**
P	0.48	**−0.05 ± 0.01**	**1.20 ± 0.08**	0.59	**0.03 ± 0.01**	**1.40 ± 0.08**
Q	0.57	**−0.18 ± 0.01**	**0.93 ± 0.06**	0.69	**−0.06 ± 0.02**	**1.28 ± 0.06**
R	0.13	**0.02 ± 0.00**	**0.23 ± 0.04**	0.10	**−0.02 ± 0.01**	**0.44 ± 0.09**

[a]The intercept terms represent the rapid adjustment response of DTR to forcing. The slope terms represent feedback and quantify the sensitivity of DTR response to changes in mean temperature. Results in bold are significant at the 5% level.

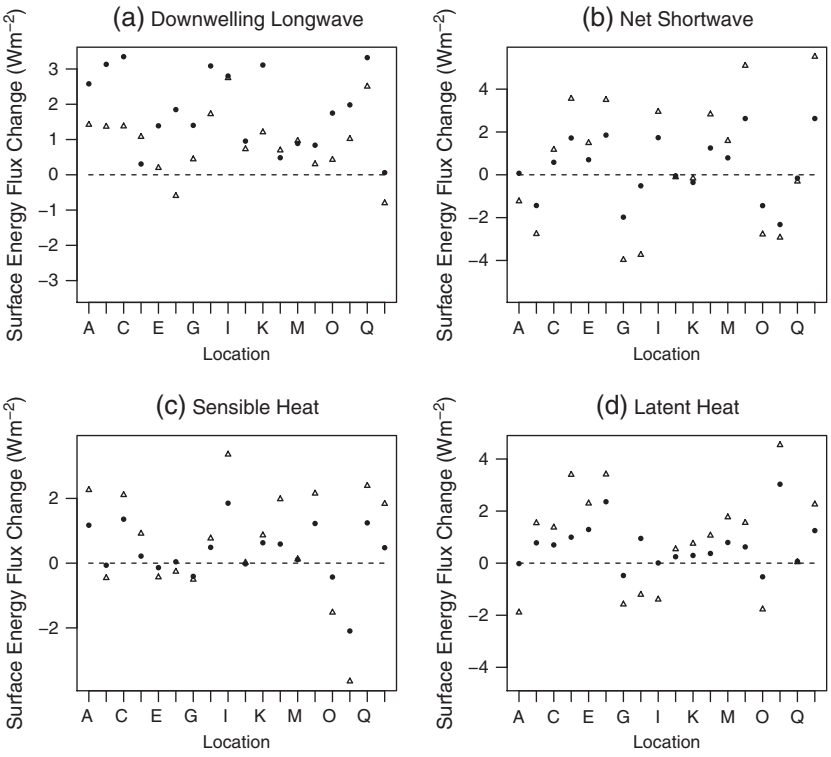

Figure 2. The ensemble mean change in surface energy fluxes for each location "A" to "R" averaged over the 3 days after CO_2 forcing. Solid circles represent the mean change in flux at the times of maximum and minimum temperature. The open triangles represent the difference in the flux changes at the times of maximum and minimum temperature (diurnal asymmetry).

smaller reduction, in energy flux at the time of maximum temperature compared to the change at the time of minimum temperature.

3. Skin Surface DTR Response to CO_2 and Solar Forcing

[18] Skin surface DTR reduced by 0.01°C averaged over the 3 days after CO_2 forcing and all locations. This change was accompanied by an increase in mean temperature of +0.11°C. The skin surface DTR response to CO_2 forcing varied between locations although there was greater variation in skin surface DTR response between the ensemble simulations at most locations than between the mean responses at different locations (Figure 1b). The skin surface DTR response included both increased and decreased DTR at all locations with the exception of only location "Q" a hot, dry location. The spread (i.e., standard deviation) in ensemble simulations at each location was caused by the perturbation of initial conditions for atmospheric temperature and humidity. This spread in DTR response was positively correlated with the spread of boundary layer height at the time of maximum temperature (+0.83), with the spread of relative humidity at the time of minimum temperature (+0.61) and with the spread of DTR in the control simulations (+0.84).

[19] Reducing total solar irradiance by 2% reduced skin surface DTR by 0.17°C averaged over the 3 days after solar forcing and all locations. Mean skin surface temperature reduced by 0.13°C. The spread in the response of DTR to solar forcing in the ensemble simulations at each location (Figure 1c) was positively correlated with the spread of boundary layer height at the time of maximum temperature (+0.90), with the spread of relative humidity at the time of minimum temperature (+0.64), and with the spread of DTR in the control simulations (+0.89).

[20] Results for the regression of the change in skin surface DTR against the mean change in skin surface temperature are summarized in Table 1 for both forcings. The regression intercept term represents a rapid adjustment response to forcing. The intercept terms for CO_2 forcing were statistically significant (at 5%) in 16 of the 18 locations, in 15 of these locations these rapid adjustments caused a reduction in DTR. For solar forcing, the intercept terms (rapid adjustments) were statistically significant (at 5%) in 12 of the 18 locations and in 7 of the 12 locations the rapid adjustments caused a reduction in DTR. The rapid adjustments to skin surface DTR had a much greater impact under CO_2 forcing than for solar forcing. For CO_2 forcing, the mean rapid adjustment, calculated using the mean regression intercept term over the 18 locations, was −0.12°C. The equivalent mean rapid adjustment for solar forcing was −0.01°C.

[21] The positive sign of the regression slope (Table 1) in all locations for CO_2 forcing, and in most locations for solar forcing, shows that feedback associated with a change in mean skin surface temperature is consistently associated with an increase in skin surface DTR. For both forcings, the regression residual component accounted for a large proportion of the change in skin surface DTR in locations where the regression had low R^2 values.

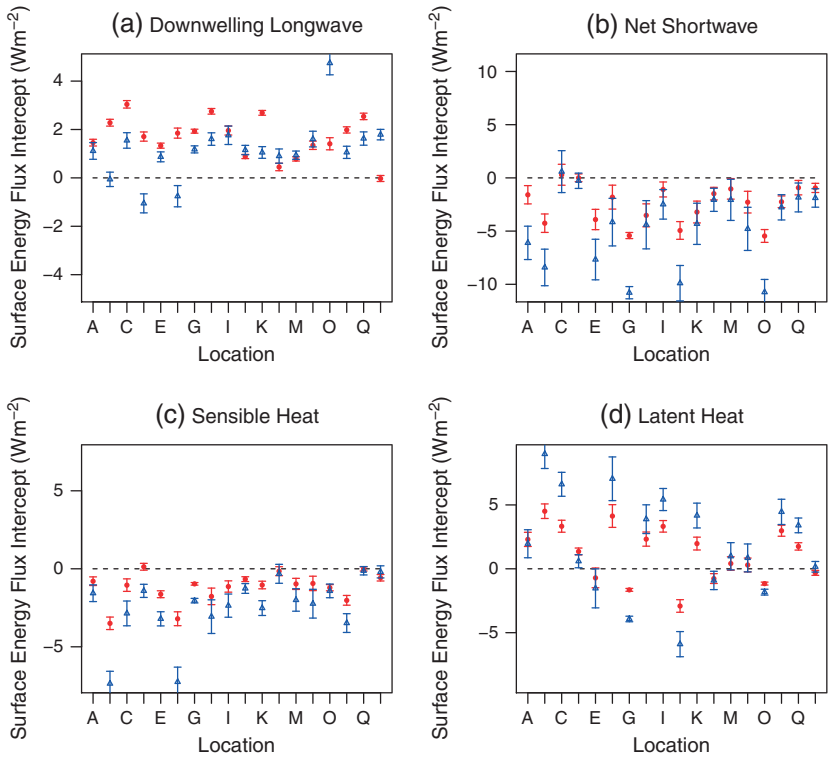

Figure 3. Intercept terms (diagnosed as rapid adjustments) from the regression of surface energy flux changes against the mean change in maximum and minimum temperatures for CO_2 forcing. Red circles represent rapid adjustments in the mean change of fluxes at the times of maximum and minimum temperature. Blue triangles represent rapid adjustments in the difference in flux changes at the times of maximum and minimum temperature (diurnal asymmetry). The intercept terms (rapid adjustments) are shown with $\pm 1\sigma$ confidence intervals.

4. Surface Energy Flux Response to CO_2 Forcing

[22] The mean value of the change in surface energy fluxes during the 3 days after CO_2 forcing, calculated for the ensemble mean change in each location, is shown in Figure 2. Downwelling LW radiation increased in all locations and the increase was greater at the time of maximum temperature than minimum temperature in 16 of the 18 locations, the exceptions being locations "F" and "R" (Figure 2a). Net SW radiation both increased and reduced across the locations due to variation in changes of cloud cover (Figure 2b). Although minimum temperatures did sometimes occur after sunrise, the change in net SW radiation is dominated by changes at the time of maximum temperature. This is apparent in Figure 2b because the difference between the diurnal asymmetry of the flux change is approximately twice the mean change in net SW radiation flux.

[23] Mean SHF and LHF increased over the 3 days after forcing in most locations (Figures 2c and 2d solid circles). Diurnal asymmetry of changes in SHF and LHF varied consistently across locations in proportion to the change in mean flux (Figures 2c and 2d open triangles). For the SHF, linear regression of diurnal asymmetry against the change in mean SHF gave a close fit to the data (R^2 0.94) and the slope of 1.84 ± 0.12 was significant at the 0.1% level. Similarly, linear regression of diurnal asymmetry in LHF against the change in mean LHF produced a slope of 1.82 ± 0.28, significant at the 0.1% level (R^2 0.72). These slope values confirm that the change in heat flux is typically greater at the time of maximum temperature compared to minimum temperature.

[24] Results for linear regression of changes in surface energy fluxes against the mean change in skin surface maximum and minimum temperatures are summarized in Table 2 and Figure 3. The intercept terms for both regression methods are shown in Figure 3. Downwelling LW radiation and net SW radiation represent the direct effect of CO_2 forcing. In 17 of the 18 locations, the intercept term was positive and significant at the 5% level for regression of the mean change in downwelling LW radiation (Figure 3a red circles). This was due to the immediate increase in atmospheric CO_2 concentrations leading to increased LW absorbed at the surface. In most locations there was a greater increase in downwelling LW radiation at the time of maximum temperature than the time of minimum temperature that acted to increase DTR, shown by the positive intercept values for the regression of diurnal asymmetry in downwelling LW radiation (Figure 3a blue triangles). In 16 of the 18 locations, the intercept term for net SW radiation reduced due to the increased atmospheric absorption of near-infrared radiation enhanced by changes in clouds and humidity which accounts for the relatively large standard errors (Figure 3b red circles).

[25] Direct forcing of downwelling LW radiation and net SW radiation caused, in addition to the rapid adjustment of DTR (section 3), rapid adjustments to SHF and LHF. The

Table 2. Linear Regression for Locations "A" to "R" After CO_2 Forcing[a]

	Net Shortwave Radiation			Downwelling Longwave Radiation			Sensible Heat Flux			Latent Heat Flux		
	Intercept (Wm^{-2})	Slope ($Wm^{-2}/°C$)	R^2	Intercept (Wm^{-2})	Slope ($Wm^{-2}/°C$)	R^2	Intercept (Wm^{-2})	Slope ($Wm^{-2}/°C$)	R^2	Intercept (Wm^{-2})	Slope ($Wm^{-2}/°C$)	R^2
(a) Mean change												
A	−1.6 ± 0.9	**11.7 ± 4.8**	0.03	**1.5 ± 0.1**	**7.9 ± 0.8**	0.32	**−0.8 ± 0.3**	**13.8 ± 1.6**	0.27	**2.3 ± 0.6**	**−16.3 ± 3.1**	0.11
B	**−4.3 ± 0.9**	**20.0 ± 4.6**	0.08	**2.3 ± 0.1**	**6.0 ± 0.8**	0.24	**−3.5 ± 0.4**	**24.3 ± 2.1**	0.38	**4.5 ± 0.6**	**−26.5 ± 3.0**	0.27
C	0.3 ± 1.0	1.3 ± 4.2	0.00	**3.0 ± 0.2**	**1.4 ± 0.7**	0.02	**−1.1 ± 0.4**	**11.1 ± 1.7**	0.16	**3.3 ± 0.5**	**−12.1 ± 2.0**	0.15
D	0.0 ± 0.4	**17.7 ± 3.4**	0.11	**1.7 ± 0.2**	**−14.4 ± 1.8**	0.24	0.1 ± 0.2	0.9 ± 2.0	0.00	**1.4 ± 0.3**	−3.7 ± 2.5	0.01
E	**−3.9 ± 1.0**	**51.6 ± 8.3**	0.16	**1.3 ± 0.1**	0.6 ± 0.9	0.00	**−1.6 ± 0.2**	**16.7 ± 1.9**	0.26	−0.7 ± 0.8	**22.4 ± 6.7**	0.05
F	−1.8 ± 1.1	**35.5 ± 8.5**	0.08	**1.9 ± 0.2**	0.0 ± 1.6	0.00	**−3.2 ± 0.4**	**31.5 ± 3.4**	0.29	**4.1 ± 0.9**	**−17.2 ± 6.7**	0.03
G	**−5.4 ± 0.3**	**96.9 ± 5.9**	0.56	**1.9 ± 0.1**	**−14.8 ± 1.7**	0.27	**−1.0 ± 0.1**	**15.7 ± 1.7**	0.29	**−1.7 ± 0.1**	**33.1 ± 2.3**	0.50
H	**−3.5 ± 1.1**	**21.7 ± 5.8**	0.06	**2.8 ± 0.1**	**2.4 ± 0.6**	0.07	**−1.8 ± 0.5**	**16.3 ± 2.8**	0.13	**2.3 ± 0.6**	**−9.9 ± 3.0**	0.05
I	−1.1 ± 0.7	**17.1 ± 2.9**	0.14	**2.0 ± 0.2**	**5.1 ± 0.8**	0.17	**−1.1 ± 0.4**	**18.1 ± 1.5**	0.41	**3.3 ± 0.5**	**−20.1 ± 1.8**	0.36
J	**−4.9 ± 0.8**	**73.3 ± 10.0**	0.20	**0.9 ± 0.1**	1.1 ± 1.0	0.00	**−0.7 ± 0.2**	**9.6 ± 1.9**	0.11	**−2.9 ± 0.5**	**47.3 ± 5.9**	0.23
K	**−3.2 ± 1.0**	**21.8 ± 6.4**	0.05	**2.7 ± 0.1**	**3.3 ± 0.6**	0.11	**−1.0 ± 0.2**	**12.8 ± 1.5**	0.25	**2.0 ± 0.5**	**−12.9 ± 3.2**	0.07
L	**−1.5 ± 0.6**	**34.0 ± 6.4**	0.12	**0.5 ± 0.2**	0.4 ± 1.7	0.00	−0.2 ± 0.3	**9.3 ± 3.1**	0.04	−0.8 ± 0.4	**14.2 ± 4.1**	0.05
M	−1.0 ± 1.0	**56.3 ± 8.8**	0.16	**0.8 ± 0.1**	**3.3 ± 0.8**	0.07	**−1.0 ± 0.4**	**33.3 ± 3.2**	0.33	0.4 ± 0.5	**11.8 ± 4.8**	0.03
N	**−2.3 ± 1.0**	**35.5 ± 6.6**	0.12	**1.4 ± 0.2**	**−3.7 ± 1.1**	0.05	**−0.9 ± 0.5**	**15.6 ± 3.0**	0.11	0.3 ± 0.5	2.4 ± 3.5	0.00
O	**−5.5 ± 0.6**	**63.9 ± 7.6**	0.25	**1.4 ± 0.3**	5.4 ± 3.2	0.01	**−1.2 ± 0.2**	**12.5 ± 2.5**	0.10	**−1.2 ± 0.1**	**10.1 ± 1.5**	0.18
P	**−2.3 ± 0.6**	**24.7 ± 5.9**	0.08	**2.0 ± 0.1**	−0.8 ± 1.4	0.00	**−2.0 ± 0.3**	**24.6 ± 3.4**	0.20	**3.0 ± 0.4**	**−17.8 ± 4.6**	0.06
Q	−0.9 ± 0.7	3.2 ± 2.7	0.01	**2.5 ± 0.1**	**3.3 ± 0.5**	0.15	0.0 ± 0.1	**5.3 ± 0.5**	0.31	**1.8 ± 0.3**	**−7.1 ± 1.2**	0.15
R	**−0.9 ± 0.4**	**37.9 ±3.9**	0.31	0.0 ± 0.1	0.9 ± 1.1	0.00	**−0.6 ± 0.2**	**11.2 ± 1.9**	0.14	−0.3 ± 0.2	**16.6 ± 1.8**	0.30
(b) Diurnal change												
A	**−6.1 ± 1.6**	**34.2 ± 8.8**	0.07	**1.1 ± 0.3**	2.2 ± 1.9	0.01	**−1.6 ± 0.5**	**26.9 ± 3.0**	0.27	2.0 ± 1.1	**−27.1 ± 6.2**	0.08
B	**−8.4 ± 1.7**	**40.1 ± 9.1**	0.08	−0.1 ± 0.3	**10.1 ± 1.6**	0.16	**−7.4 ± 0.8**	**49.0 ± 4.2**	0.39	**9.0 ± 1.1**	**−52.9 ± 6.0**	0.27
C	0.6 ± 2.0	2.7 ± 8.4	0.00	**1.6 ± 0.3**	−0.8 ± 1.4	0.00	**−2.9 ± 0.8**	**22.8 ± 3.4**	0.18	**6.6 ± 0.9**	**−24.1 ± 4.0**	0.14
D	−0.3 ± 0.7	**39.4 ± 6.7**	0.14	**−1.1 ± 0.4**	**22.0 ± 3.6**	0.14	**−1.4 ± 0.4**	**24.0 ± 3.9**	0.15	0.6 ± 0.5	**28.9 ± 4.7**	0.15
E	**−7.7 ± 1.9**	**102.4 ± 16.5**	0.15	**0.9 ± 0.2**	**−7.5 ± 1.8**	0.08	**−3.2 ± 0.5**	**31.0 ± 3.9**	0.23	−1.5 ± 1.5	**42.8 ± 13.2**	0.05
F	−4.2 ± 2.2	**74.3 ± 17.0**	0.08	−0.8 ± 0.4	1.6 ± 3.3	0.00	**−7.3 ± 1.0**	**67.8 ± 7.2**	0.29	**7.1 ± 1.7**	**−35.3 ± 13.0**	0.03
G	**−10.8 ± 0.6**	**192.0 ± 11.7**	0.56	**1.2 ± 0.2**	**−20.7 ± 3.0**	0.18	**−2.0 ± 0.2**	**43.2 ± 3.0**	0.49	**−3.9 ± 0.2**	**66.1 ± 4.4**	0.51
H	−4.4 ± 2.3	4.8 ± 12.1	0.00	**1.6 ± 0.3**	0.9 ± 1.4	0.00	**−3.1 ± 1.1**	**27.6 ± 5.8**	0.10	**3.9 ± 1.1**	**−36.7 ± 6.0**	0.15
I	−2.5 ± 1.4	**32.9 ± 5.7**	0.14	**1.8 ± 0.4**	**6.0 ± 1.6**	0.06	**−2.4 ± 0.7**	**34.6 ± 3.0**	0.38	**5.4 ± 0.9**	**−41.3 ± 3.5**	0.39
J	**−9.9 ± 1.7**	**146.6 ± 19.9**	0.20	**1.2 ± 0.2**	**−6.3 ± 2.3**	0.03	**−1.3 ± 0.3**	**19.2 ± 3.7**	0.11	**−5.9 ± 1.0**	**96.4 ± 11.8**	0.24
K	**−4.3 ± 1.9**	**31.8 ± 12.2**	0.03	**1.1 ± 0.2**	1.2 ± 1.5	0.00	**−2.5 ± 0.5**	**25.9 ± 3.0**	0.26	**4.2 ± 1.0**	**−26.2 ± 6.1**	0.08
L	−2.1 ± 1.1	**60.8 ± 11.7**	0.11	**0.9 ± 0.3**	−2.6 ± 3.2	0.00	−0.3 ± 0.6	**28.6 ± 6.5**	0.08	−0.9 ± 0.7	**24.5 ± 7.7**	0.04
M	−2.1 ± 1.9	**112.5 ± 17.5**	0.16	**0.9 ± 0.2**	0.8 ± 1.5	0.00	**−2.0 ± 0.7**	**65.3 ± 6.5**	0.32	1.0 ± 1.1	**24.2 ± 9.7**	0.03
N	**−4.8 ± 2.0**	**71.4 ± 13.2**	0.12	**1.6 ± 0.3**	**−9.4 ± 2.1**	0.08	**−2.2 ± 0.9**	**31.7 ± 6.0**	0.12	0.9 ± 1.1	5.0 ± 7.1	0.00
O	**−10.7 ± 1.2**	**126.6 ± 15.1**	0.25	**4.8 ± 0.5**	**−68.7 ± 6.1**	0.37	**−1.4 ± 0.4**	−1.7 ± 5.5	0.00	**−1.8 ± 0.2**	0.9 ± 2.9	0.00
P	**−2.8 ± 1.2**	**54.7 ± 12.8**	0.08	**1.1 ± 0.3**	**12.5 ± 2.7**	0.09	**−3.5 ± 0.6**	**57.7 ± 6.5**	0.27	**4.5 ± 1.0**	**−27.3 ± 10.6**	0.03
Q	−1.8 ± 1.4	6.4 ± 5.5	0.01	**1.6 ± 0.3**	**3.7 ± 1.1**	0.05	−0.1 ± 0.3	**10.6 ± 1.1**	0.31	**3.4 ± 0.6**	**−14.1 ± 2.3**	0.15
R	**−1.9 ± 0.9**	**78.6 ± 7.8**	0.32	**1.8 ± 0.2**	**−27.5 ± 2.0**	0.48	−0.2 ± 0.4	**21.6 ± 3.5**	0.15	0.2 ± 0.4	**22.3 ± 3.8**	0.14

[a](a) Mean Change: Mean change in surface energy flux at the time of maximum and minimum temperature against the mean change in maximum and minimum temperatures. (b) Diurnal Change: Diurnal asymmetry in the surface energy change against the mean change in maximum and minimum temperatures. The intercept terms represent the rapid adjustment response of surface fluxes to forcing. The slope terms represent feedback and quantify the sensitivity of flux changes to changes in mean temperature. Results in bold are significant at the 5% level.

regression intercept terms (Table 2) represent the rapid adjustment of surface heat fluxes in the 3 days after CO_2 forcing. Rapid adjustment of the mean change in SHF reduced SHF in 17 of the 18 locations (Figure 3c red circles) and was significant at the 5% level in 15 locations. Rapid adjustment of the diurnal asymmetry in SHF (Figure 3c blue triangles) was closely correlated with the rapid adjustment of the mean change in SHF (correlation coefficient +0.95). In almost all locations, the reduction in SHF was greater at the time of maximum temperature than minimum temperature.

[26] The rapid adjustment of the mean change in LHF involved an increase in LHF in twelve locations, ten of which were significant at the 5% level (Figure 3d red circles). Similar to the SHF, rapid adjustment of the diurnal asymmetry in LHF (Figure 3d blue triangles) was strongly correlated with the rapid adjustment of the mean change in LHF (correlation coefficient +0.98) and the LHF at the time of maximum temperature was more sensitive to CO_2 forcing than the LHF at the time of minimum temperature. Rapid adjustments for SHF and LHF were negatively correlated with one another in locations where the LHF rapid adjustment was positive. This applied to rapid adjustments of mean changes and rapid adjustments in the diurnal asymmetry of flux changes. Furthermore, the rapid adjustment for LHF was greater in absolute terms than the rapid adjustment for SHF in these locations.

[27] The rapid adjustments in surface energy fluxes and the direct effects of forcing help interpret the rapid adjustment in DTR. The increase in surface downwelling LW radiation, being greater at the time of maximum temperature than minimum temperature acted to increase DTR. The rapid reduction in surface net SW radiation, enhanced by changes in clouds and humidity, opposed the effect of the downwelling LW radiation resulting in a reduction in net radiation at the surface. This change in net radiation drove the rapid adjustments to SHF, LHF and DTR. In most locations, the rapid adjustment in LHF opposed the rapid adjustment in SHF. The rapid adjustment in DTR (Table 1) was most strongly correlated with the rapid adjustment of

Table 3. Linear Regression for Locations "A" to "R" After Solar Forcing[a]

	Net Shortwave Radiation			Downwelling Longwave Radiation			Sensible Heat Flux			Latent Heat Flux		
	Intercept (Wm^{-2})	Slope ($Wm^{-2}/°C$)	R^2	Intercept (Wm^{-2})	Slope ($Wm^{-2}/°C$)	R^2	Intercept (Wm^{-2})	Slope ($Wm^{-2}/°C$)	R^2	Intercept (Wm^{-2})	Slope ($Wm^{-2}/°C$)	R^2
(a) Mean change												
A	**−2.8 ± 0.9**	**21.4 ± 3.5**	0.14	**1.6 ± 0.2**	**7.9 ± 0.7**	0.39	−0.5 ± 0.4	**12.9 ± 1.4**	0.27	**−4.5 ± 0.6**	**−13.2 ± 2.4**	0.12
B	**−1.9 ± 0.9**	**31.6 ± 3.2**	0.30	**0.7 ± 0.2**	**7.9 ± 0.6**	0.44	−0.4 ± 0.4	**25.8 ± 1.5**	0.58	**−2.6 ± 0.5**	**−14.5 ± 1.8**	0.23
C	**−3.2 ± 0.8**	**22.1 ± 3.3**	0.16	0.1 ± 0.1	**1.9 ± 0.6**	0.04	−0.3 ± 0.3	**18.9 ± 1.4**	0.44	**−2.4 ± 0.4**	**−8.6 ± 1.6**	0.11
D	**−1.4 ± 0.4**	**29.9 ± 6.6**	0.08	0.1 ± 0.2	−1.5 ± 2.9	0.00	0.0 ± 0.2	**15.6 ± 3.7**	0.07	**−1.3 ± 0.3**	0.5 ± 4.9	0.00
E	−0.6 ± 1.6	**36.9 ± 9.5**	0.06	−0.2 ± 0.2	**2.2 ± 1.1**	0.02	0.6 ± 0.3	**13.1 ± 1.9**	0.17	−1.4 ± 1.2	**16.2 ± 6.8**	0.02
F	0.3 ± 1.3	**47.0 ± 10.2**	0.09	−0.2 ± 0.2	**−3.7 ± 1.5**	0.02	**1.1 ± 0.4**	**28.9 ± 3.5**	0.23	−2.0 ± 1.0	−8.2 ± 8.1	0.00
G	0.1 ± 0.4	**82.6 ± 7.4**	0.36	**−0.7 ± 0.1**	**−13.3 ± 2.3**	0.14	**−0.4 ± 0.1**	**12.2 ± 2.0**	0.14	−0.1 ± 0.1	**27.3 ± 2.5**	0.36
H	−0.4 ± 1.3	**23.8 ± 4.6**	0.10	−0.2 ± 0.1	**1.5 ± 0.4**	0.05	0.1 ± 0.6	**18.8 ± 2.2**	0.24	**−1.2 ± 0.6**	**−7.9 ± 2.1**	0.06
I	**−3.2 ± 0.7**	**14.8 ± 2.7**	0.11	**0.7 ± 0.1**	**6.6 ± 0.5**	0.40	0.0 ± 0.4	**16.9 ± 1.3**	0.40	**−4.7 ± 0.5**	**−24.9 ± 1.9**	0.42
J	−0.4 ± 1.3	**52.3 ± 11.3**	0.09	**−0.7 ± 0.1**	−1.3 ± 1.0	0.01	−0.6 ± 0.3	1.0 ± 2.9	0.00	0.7 ± 0.6	**50.3 ± 5.7**	0.26
K	−0.6 ± 1.0	**31.5 ± 5.1**	0.14	0.1 ± 0.1	**2.9 ± 0.5**	0.15	**−1.4 ± 0.3**	**9.2 ± 1.4**	0.15	**−1.4 ± 0.5**	**−9.0 ± 2.3**	0.06
L	**−4.3 ± 1.0**	−2.1 ± 11.6	0.00	−0.3 ± 0.2	−2.5 ± 2.1	0.01	−0.5 ± 0.4	**12.7 ± 5.1**	0.03	**−3.4 ± 0.8**	**−18.8 ± 9.2**	0.02
M	**6.5 ± 1.4**	**107.9 ± 7.3**	0.50	**−0.8 ± 0.2**	**−3.9 ± 0.8**	0.10	**3.1 ± 0.5**	**42.9 ± 2.6**	0.54	0.7 ± 0.8	**37.3 ± 4.1**	0.27
N	**3.7 ± 0.5**	**102.8 ± 5.7**	0.59	**−0.4 ± 0.1**	**−2.9 ± 1.0**	0.03	0.2 ± 0.2	**22.9 ± 2.7**	0.24	**2.3 ± 0.3**	**49.0 ± 3.2**	0.52
O	0.0 ± 0.6	**19.5 ± 9.0**	0.02	−0.3 ± 0.3	**11.6 ± 3.9**	0.04	**0.6 ± 0.3**	**17.6 ± 3.8**	0.09	0.1 ± 0.1	−1.6 ± 1.5	0.00
P	**−4.8 ± 0.9**	**19.9 ± 6.4**	0.04	0.1 ± 0.2	−0.4 ± 1.7	0.00	0.6 ± 0.4	**27.9 ± 3.0**	0.28	**−6.0 ± 0.7**	**−27.3 ± 5.0**	0.11
Q	**−5.6 ± 1.1**	−1.8 ± 3.8	0.00	−0.1 ± 0.2	**2.9 ± 0.7**	0.08	**−1.7 ± 0.3**	**4.4 ± 0.9**	0.09	**−2.8 ± 0.4**	**−10.5 ± 1.3**	0.22
R	**−1.3 ± 0.5**	**25.7 ± 6.3**	0.06	0.1 ± 0.2	−2.0 ± 2.3	0.00	**−0.9 ± 0.2**	**−8.3 ± 2.7**	0.04	−0.2 ± 0.2	**23.6 ± 2.6**	0.24
(b) Diurnal change												
A	**−10.1 ± 1.9**	**22.0 ± 7.2**	0.04	**1.9 ± 0.4**	**10.8 ± 1.5**	0.18	**−2.8 ± 0.8**	**22.7 ± 2.8**	0.22	**−11.7 ± 1.3**	**−40.0 ± 4.7**	0.24
B	**−3.9 ± 1.8**	**63.2 ± 6.4**	0.30	**1.9 ± 0.3**	**15.9 ± 1.2**	0.42	−0.7 ± 0.8	**52.1 ± 2.9**	0.58	**−5.3 ± 1.0**	**−28.9 ± 3.5**	0.23
C	**−6.4 ± 1.5**	**44.2 ± 6.6**	0.16	**−0.6 ± 0.3**	1.3 ± 1.1	0.00	−0.7 ± 0.6	**38.1 ± 2.8**	0.44	**−4.8 ± 0.7**	**−17.3 ± 3.2**	0.11
D	**−3.1 ± 0.9**	**52.9 ± 13.5**	0.06	−0.3 ± 0.5	2.9 ± 7.0	0.00	0.3 ± 0.5	**38.5 ± 7.2**	0.11	**−3.2 ± 0.6**	4.7 ± 9.3	0.00
E	−1.2 ± 3.3	**74.1 ± 19.1**	0.06	**−1.3 ± 0.3**	−3.1 ± 1.9	0.01	0.9 ± 0.7	**25.4 ± 3.9**	0.16	−3.2 ± 2.3	**30.5 ± 13.6**	0.02
F	0.1 ± 2.4	**88.6 ± 18.8**	0.09	−0.5 ± 0.5	2.1 ± 4.0	0.00	**1.9 ± 0.8**	**64.6 ± 5.9**	0.34	**−3.9 ± 1.9**	−14.0 ± 15.4	0.00
G	0.3 ± 0.8	**167.2 ± 14.5**	0.38	**−0.5 ± 0.2**	**−12.3 ± 3.6**	0.05	−0.2 ± 0.2	**37.8 ± 4.4**	0.26	0.1 ± 0.3	**63.2 ± 4.8**	0.44
H	−0.5 ± 2.5	**51.3 ± 9.2**	0.11	**−0.6 ± 0.3**	**4.9 ± 1.0**	0.09	0.4 ± 1.2	**39.8 ± 4.3**	0.26	**−2.7 ± 1.2**	**−10.7 ± 4.5**	0.02
I	**−8.1 ± 1.4**	**29.9 ± 5.1**	0.12	−0.5 ± 0.3	**14.8 ± 1.3**	0.35	−0.5 ± 0.7	**34.2 ± 2.6**	0.41	**−11.5 ± 1.0**	**−50.4 ± 3.7**	0.43
J	−0.8 ± 2.5	**105.5 ± 22.5**	0.09	**−0.9 ± 0.3**	**−8.7 ± 2.3**	0.06	−1.1 ± 0.6	2.5 ± 5.7	0.00	1.5 ± 1.3	**100.0 ± 11.5**	0.25
K	**−12.4 ± 2.0**	6.1 ± 10.1	0.00	**−0.9 ± 0.3**	**−2.5 ± 1.2**	0.02	**−3.3 ± 0.5**	**17.8 ± 2.6**	0.16	**−5.3 ± 0.9**	**−25.8 ± 4.6**	0.12
L	**−8.8 ± 1.9**	−8.9 ± 21.5	0.00	−0.7 ± 0.4	**−15.5 ± 4.5**	0.05	−0.8 ± 0.9	**21.3 ± 10.4**	0.02	**−6.8 ± 1.5**	**−35.6 ± 17.3**	0.02
M	**13.1 ± 2.9**	**215.8 ± 14.5**	0.50	0.2 ± 0.3	**3.6 ± 1.3**	0.03	**6.4 ± 1.1**	**88.2 ± 5.4**	0.55	1.1 ± 1.6	**73.6 ± 8.2**	0.26
N	**7.5 ± 1.0**	**205.6 ± 11.6**	0.58	**−0.8 ± 0.2**	**−8.2 ± 2.0**	0.07	0.4 ± 0.5	**45.3 ± 5.3**	0.25	**4.5 ± 0.6**	**96.6 ± 6.4**	0.50
O	0.0 ± 1.2	**40.3 ± 18.5**	0.02	**−1.0 ± 0.5**	4.1 ± 7.2	0.00	−0.4 ± 0.5	0.8 ± 7.3	0.00	**−0.9 ± 0.2**	**−32.7 ± 3.4**	0.29
P	**−8.4 ± 1.7**	**29.2 ± 12.2**	0.02	0.3 ± 0.4	**12.1 ± 3.1**	0.06	**1.9 ± 0.8**	**68.7 ± 5.6**	0.39	**−12.1 ± 1.5**	**−68.1 ± 10.8**	0.15
Q	**−11.1 ± 2.2**	−3.5 ± 7.7	0.00	−0.3 ± 0.4	**4.6 ± 1.4**	0.05	**−3.4 ± 0.5**	**8.9 ± 1.9**	0.09	**−5.6 ± 0.8**	**−20.9 ± 2.7**	0.22
R	**−3.0 ± 0.9**	**44.5 ± 12.8**	0.05	−0.4 ± 0.4	−6.5 ± 4.8	0.01	**−1.7 ± 0.4**	−5.0 ± 5.6	0.00	**−1.0 ± 0.4**	**40.4 ± 5.7**	0.17

[a](a) Mean Change: Mean change in surface energy flux at the time of maximum and minimum temperature against the mean change in maximum and minimum temperatures. (b) Diurnal Change: Diurnal asymmetry in the surface energy change against the mean change in maximum and minimum temperatures. The intercept terms represent the rapid adjustment response of surface fluxes to forcing. The slope terms represent feedback and quantify the sensitivity of flux changes to changes in mean temperature. Results in bold are significant at the 5% level.

diurnal asymmetry in SHF and LHF (Table 2, Figures 3c and 3d, blue triangles) (correlation coefficients +0.68 and −0.68 respectively). Only in locations where rapid adjustments in SHF and LHF were relatively small (locations "D", "L", and "R") did DTR not reduce by a significant amount.

5. Surface Energy Flux Response to Solar Forcing

[28] The mean value of the change in surface energy fluxes during the 3 days after forcing, calculated separately for the ensemble mean in each location, is shown in Figure 4. Downwelling LW radiation reduced in all but four locations and the reduction was greater at the time of maximum temperature than minimum temperature in 15 of the 18 locations (Figure 4a). Net SW radiation reduced across all locations and, as expected, the change was dominated by changes at the time of maximum temperature (Figure 4b).

[29] Mean SHF and LHF reduced over the 3 days after forcing in most locations (Figures 4c and 4d, respectively). Diurnal asymmetry of changes in SHF and LHF varied in proportion to the change in mean fluxes across the 18 locations. For the SHF, linear regression of diurnal asymmetry in the SHF change (Figure 4c open triangles) against the change in mean SHF (Figure 4c solid circles) gave a close fit to the data (R^2 0.99) and the slope of 2.03 ± 0.06 was significant at the 0.1% level. Similarly for the LHF, linear regression of diurnal asymmetry in the LHF change (Figure 4d open triangles) against the change in mean LHF (Figure 4d solid circles) gave a close fit to the data (R^2 0.95) and the slope of 1.81 ± 0.10 was significant at the 0.1% level. For solar forcing, as with CO_2 forcing, the change in SHF and LHF is typically greater at the time of maximum temperature than minimum temperature.

[30] Results for the regression of mean changes in surface fluxes and the regression of diurnal asymmetry in surface flux changes are summarized in Table 3 and Figure 5 for solar forcing. The intercept term for downwelling LW radiation shows the behavior of the rapid adjustment varied between locations. In the seven locations where the intercept

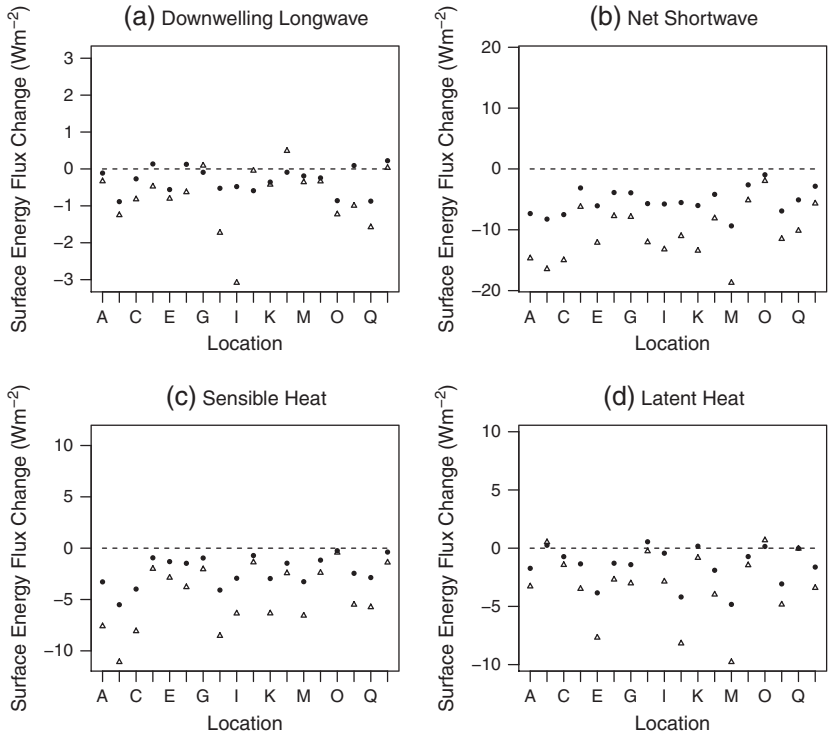

Figure 4. The ensemble mean change in surface energy fluxes for each location "A" to "R" averaged over the 3 days after solar forcing. Solid circles represent the mean change in flux at the times of maximum and minimum temperature. The open triangles represent the difference in the flux changes at the times of maximum and minimum temperature (diurnal asymmetry).

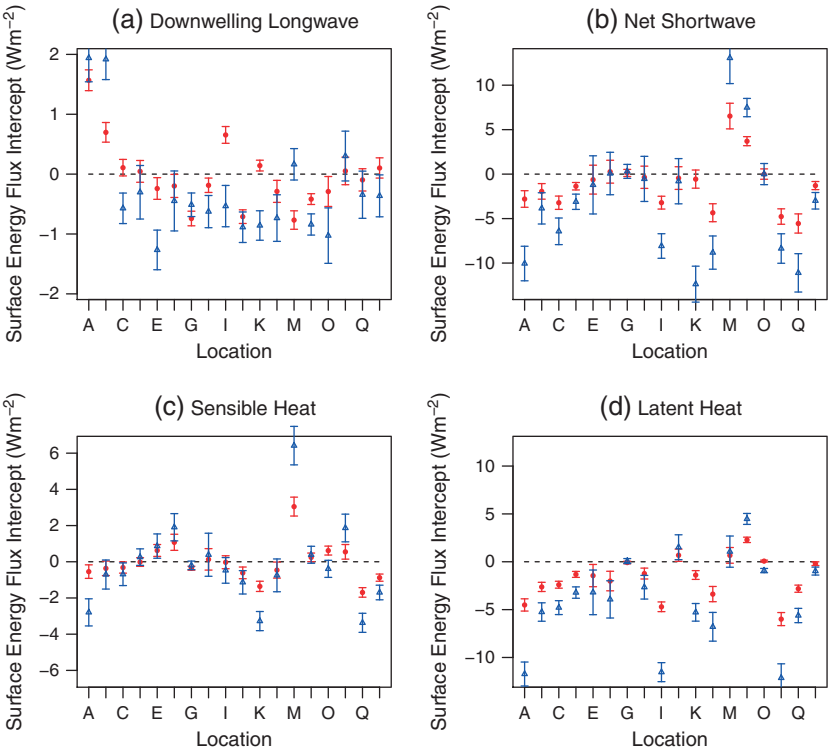

Figure 5. Intercept terms (diagnosed as rapid adjustments) from the regression of surface energy flux changes against the mean change in maximum and minimum temperatures for solar forcing. Red circles represent rapid adjustments in the mean change of fluxes at the times of maximum and minimum temperature. Blue triangles represent rapid adjustments in the difference in flux changes at the times of maximum and minimum temperature (diurnal asymmetry). The intercept terms (rapid adjustments) are shown with $\pm 1\sigma$ confidence intervals.

was significant (Table 3 and Figure 5a red circles) four of the intercepts show downwelling LW radiation reduced and three increased. The intercept term for net SW radiation represents the direct effect of solar forcing. In 13 of the 18 locations the intercept term was negative for net SW radiation due to the reduction in total solar irradiance (Figure 5b red circles). The changes in net SW radiation were modified by changes in clouds and humidity, which accounts for the increase in surface net SW radiation in some locations and for the relatively large standard errors.

[31] Direct forcing of net SW radiation caused rapid adjustments to SHF and LHF in the 3 days after solar forcing, represented by the regression intercept terms (Table 3, Figures 5c and 5d). Rapid adjustment of the mean change in SHF reduced SHF in 11 of the 18 locations (Figure 5c red circles) although in only four of these locations were the changes significant at the 5% level. Rapid adjustment of the diurnal asymmetry in the SHF change (Figure 5c blue triangles) was closely correlated with the rapid adjustment in mean change SHF (correlation coefficient +0.96). In almost all locations, the reduction in SHF was greater at the time of maximum temperature than minimum temperature. Rapid adjustment of the mean change in LHF reduced the LHF in 14 locations and 10 of these had significant intercept terms. Similar to the SHF, rapid adjustment of the diurnal asymmetry in the LHF change was strongly correlated with the rapid adjustment of the mean change in LHF (correlation coefficient +0.98) and the LHF at the time of maximum temperature was more sensitive than at the time of minimum temperature. Rapid adjustments for SHF and LHF were not strongly correlated across locations (correlation coefficient +0.21) unlike for CO_2 forcing.

[32] The rapid adjustments to DTR and surface energy fluxes varied more widely between locations with solar forcing compared to CO_2 forcing. A clear relationship between the rapid adjustment of DTR and diurnal asymmetry in changes to net SW radiation and SHF is still apparent, however, for solar forcing. The rapid adjustments to DTR across the 18 locations were correlated with diurnal asymmetry in changes to net SW radiation and SHF with correlation coefficients +0.62 and +0.67, respectively. The influence of the rapid reductions in LHF, found in most locations, is likely as important as the rapid adjustments to SHF but was confounded with changes in cloud cover and more strongly dependent on local land surface conditions making it more difficult to generalize temperature and LHF relationships across locations.

6. Rapid Adjustment of DTR for Skin Surface and Surface Air

[33] The skin surface DTR response to CO_2 forcing averaged over the 3 days and all locations after forcing (−0.01°C) included a large contribution from rapid adjustments (−0.12°C). For solar forcing, the mean response of skin surface DTR (−0.17°C) included a smaller contribution from rapid adjustments (−0.01°C). The key role played by the rapid adjustment of DTR under CO_2 forcing and its dependence on the surface characteristics and meteorology of each location is demonstrated by linear regression of the change in skin surface DTR against the mean change in skin surface maximum and minimum temperatures across locations (Table 4 and Figure 6). The regression provided a poor fit to the change in DTR for CO_2 forcing (R^2 0.06). The fit to data improved when the DTR rapid adjustment (Table 1) was deducted from the change in DTR in each location (R^2 0.63). The intercept term of this regression is statistically indistinguishable from zero, consistent with removal of the rapid adjustment. The slope term, which represents the sensitivity of the change in DTR to temperature related feedback, is statistically equivalent to the regression slope calculated for solar forcing (Figure 6). This suggests that the sensitivity of DTR to the change in mean temperature may be the same for both forcings and the same in different locations. The variation in rapid adjustments between different forcings and locations may account for a significant proportion of the variation in DTR response between the forcings and locations. Variations in land-atmosphere coupling strength, which vary regionally and influence the interseasonal variability in DTR [*Zhang et al*., 2009; *Zhang et al*., 2011; *Steeneveld et al*., 2011], are likely to affect the

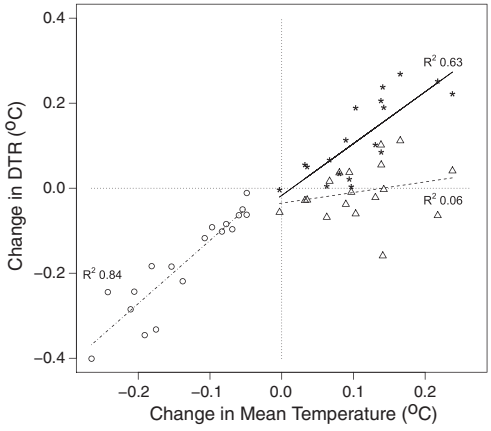

Figure 6. Regression of the mean change in DTR at each location (*y*-axis) against the mean change in maximum and minimum temperatures (*x*-axis) for solar forcing (open circles), CO_2 forcing (open triangles) and CO_2 forcing with the DTR rapid adjustment deducted from the change in DTR (asterisk). The regression lines are represented by the dot-dashed line for solar forcing, dashed line for CO_2 forcing and solid line for CO_2 forcing with the DTR rapid adjustment deducted.

Table 4. Linear Regression of the Change in DTR (With and Without Deduction of the Rapid Adjustment at Each Location) Against the Mean Change in Maximum and Minimum Temperatures (ΔT)[a]

	CO_2 Forcing			Solar Forcing		
	R^2	Intercept (°C)	Slope (°C/°C)	R^2	Intercept (°C)	Slope (°C/°C)
ΔDTR ~ ΔT	0.06	-0.04 ± 0.03	0.25 ± 0.26	0.84	0.03 ± 0.02	$\mathbf{1.49 \pm 0.16}$
ΔDTR less rapid adjustment ~ ΔT	0.63	-0.02 ± 0.03	$\mathbf{1.22 \pm 0.23}$	0.47	0.01 ± 0.05	$\mathbf{1.30 \pm 0.35}$

[a]The slope terms represent feedback and quantify the sensitivity of flux changes to changes in mean temperature. Results in bold are significant at the 5% level.

strength of DTR rapid adjustments and will likely play a role in the regional variation of DTR responses.

[34] Like skin surface temperatures, diurnal variations in surface air temperatures are driven by changes in surface energy fluxes although have a weaker linkage to surface fluxes and typically a smaller DTR. Surface air temperatures are also subject to nonlinear processes, particularly in the evolution of the nocturnal boundary layer, that redistribute heat within the boundary layer and strongly influence the vertical profile of temperature for near surface air [e.g., *Walters et al*., 2007]. For surface air temperatures, the mean DTR averaged over the 3 days after CO_2 forcing in all locations, reduced by 0.03°C accompanied by an increase in daily mean temperature of +0.09°C. For solar forcing, the mean change in surface air DTR reduced by 0.06°C accompanied by a reduction in daily mean temperature of 0.09°C.

[35] Rapid adjustments of DTR for surface air, calculated by regression against the change in skin surface mean temperature, behaved differently for the two forcings. For CO_2 forcing, the rapid adjustments of DTR for surface air were strongly correlated across the locations with the rapid adjustments of DTR for the skin surface (correlation coefficient +0.84). The rapid adjustments of DTR for surface air were 44% of the rapid adjustments of DTR for the skin surface. In contrast for solar forcing, rapid adjustments of DTR for surface air were weakly correlated with the rapid adjustments of DTR for the skin surface (correlation coefficient +0.35) and were only 37% of the magnitude of the rapid adjustments of DTR for the skin surface.

7. Discussion and Conclusions

[36] Our modeled changes in DTR with CO_2 forcing are consistent with previous modeling studies in terms of the relationships between DTR and surface fluxes [e.g., *Cao et al*., 1992; *Stenchikov and Robock*, 1995; *Watterson*, 1997]. Increased atmospheric absorption of near-infrared radiation reduced net SW radiation and acted to reduce DTR, as did increased SHF and LHF. Previous investigations into the response of DTR to solar forcing showed the change in DTR is positively correlated with changes in solar radiation [e.g., *Watterson*, 1997; *Stone and Weaver*, 2003] and is damped by changes in the hydrological cycle [e.g., *Betts*, 2004]. Despite limitations of the idealized boundary conditions and the absence of large-scale atmospheric circulation our experimental design reproduced these characteristics. Our results, however, are sensitive to uncertainties in SCCM parameters, which in some cases are model heuristics rather than true physical representations [e.g., *McNider et al*., 2005]. Perturbation of the parameter values controlling skin surface and surface air temperatures, or simulations using different land surface models could help quantify this uncertainty.

[37] Our diagnosis of skin surface DTR rapid adjustments in response to simulated CO_2 and solar forcings provides a new example of rapid adjustments. The large reduction in skin surface DTR found for CO_2 forcing and the smaller reduction for solar forcing mirrors the impact of rapid adjustments on precipitation for the two forcings [*Andrews et al*., 2009]. The rapid adjustment increase in LHF found in the majority of locations for CO_2 forcing is consistent with the increase in surface LHF over land mapped by *Bala et al*. [2010] although our single column sample size is relatively small.

[38] Comparing modeled trends in surface SW radiation, downwelling LW radiation, and DTR for surface air over land for the period 1950–1999, *Zhou et al*. [2010] found the observed trend in DTR to be correlated with interannual variations in downwelling SW radiation and only weakly correlated with downwelling LW radiation. Our results confirm that skin surface DTR is also sensitive to changes in surface solar radiation and suggest that solar forcing is associated with relatively small but geographically variable rapid adjustments of DTR. We also find that skin surface DTR is sensitive to diurnal variation in downwelling LW radiation due to CO_2 forcing and that skin surface DTR is reduced by rapid adjustments in surface SHF and LHF. While global dimming and subsequent brightening of surface shortwave radiation is most closely correlated with the observed trend in DTR for surface air [*Zhou et al*., 2010], our results suggest additional contributions from diurnal variation in the trend of downwelling LW radiation and rapid reductions in DTR associated with CO_2 forcing.

[39] **Acknowledgments.** We thank the R software development team and the developers of the NCAR SCCM climate model. The Ph.D. studentship of Lawrence Jackson was funded by the Natural Environment Research Council (NERC) with further support from the Integrated Assessment of Geo-engineering Proposals (IAGP) grant (EP/I014721/1) from the Engineering and Physical Sciences Research Council (EPSRC) and NERC. Piers Forster was supported by a Royal Society Wolfson Merit Award. Finally, we thank Richard McNider, John Nielsen-Gammon and two anonymous reviewers for reviewing this manuscript and for the improvements resulting from their comments and suggestions.

References

Andrews, T., P. M. Forster, and J. M. Gregory (2009), A surface Energy Perspective on Climate Change, *J. Climate 22*, 2557–2570, doi:10.1175/2008JCLI2759.1.

Bala, G., K. Caldeira and R. Nemani (2010), Fast versus slow response in climate change: implications for the global hydrological cycle, *Clim Dynam*, *35*(2–3), 423–434.

Betts, A. K. (2004), Understanding hydrometeorology using global models, *Bull. Am. Meteorol. Soc.*, *85*(11), 1673–1688, doi:10.1175/BAMS-85-11-1673.

Braganza, K., D. J. Karoly, and J. M. Arblaster (2004), Diurnal temperature range as an index of global climate change during the twentieth century, *Geophys. Res. Lett.*, *31*, L13217, doi:10.1029/2004GL019998.

Cao, H. X., J. F. B. Mitchell, and J. R. Lavery (1992), Simulated Diurnal Range and Variability of Surface Temperature in a Global Model for Present and Doubled CO_2 Climates, *J. Climate*, *5*, 920–943.

Collins, W. D., et al. (2004), Description of the NCAR Community Atmosphere Model (CAM 3.0), *NCAR Technical Note NCAR/TN-464 + STR*, National Center for Atmospheric Research, Boulder, Colorado.

Dai, A., K. E. Trenberth, and T. R. Karl (1999), Effects of clouds, soil moisture, precipitation and water vapour on diurnal temperature range, *J. Climate*, *12*, 2451–2473.

Dong, B., J. M. Gregory and R. T. Sutton (2009), Understanding Land-Sea Warming Contrast in Response to Increasing Greenhouse Gases. Part I: Transient Adjustment, *J. Climate*, *22*(11), 3079–3097, doi: 10.1175/2009JCLI2652.1.

Doutriaux-Boucher, M., M. J. Webb, J. M. Gregory, and O. Boucher (2009), Carbon dioxide induced stomatal closure increases radiative forcing via a rapid reduction in low cloud, *Geophys. Res. Lett.*, *36*, L02703, doi:10.1029/2008GL036273.

Gregory, J., and M. Webb (2008), Tropospheric Adjustment Induces a Cloud Component in CO2 Forcing, *J. Climate*, *21*, 58–71.

Hack, J. J., J. E. Truesdale, J. A. Pedretti and J. C. Petch (2004), SCAM User's Guide, http://www.ccsm.ucar.edu/models/atm-cam/docs/scam

Hansen J., M. Sato and R. Ruedy (1995), Long-term changes of the diurnal temperature cycle: implications about mechanisms of global climate change, *Atmos Res*, *37*(1–3), 175–209.

McNider, R. T., W. M. Lapenta, A. P. Biazar, G. J. Jedlovec, R. J. Suggs and J. Pleim (2005), Retrieval of Model Grid-Scale Heat Capacity Using

Geostationary Satellite Products. Part I: First Case-Study Application, *J. Appl. Meteorol.*, *44*, 1346–1360.

Oleson, K. W., et al. (2004), Technical Description of the Community Land Model (CLM), *NCAR Technical Note NCAR/TN-461 + STR*, National Center for Atmospheric Research, Boulder, Colorado.

Steeneveld, G. J., A. A. M. Holtslag, R. T. McNider, and R. A. Pielke Sr. (2011), Screen level temperature increase due to higher atmospheric carbon dioxide in calm and windy nights revisited, *J. Geophys. Res.*, *116*, D02122, doi:10.1029/2010JD014612.

Stenchikov, G. L. and A. Robuck (1995), Diurnal asymmetry of climatic response to increased CO_2 and aerosols: Forcings and feedbacks, *J. Geophys. Res.*, *100*(D12), 26211–26227.

Stone, D. A. and A. J. Weaver (2003), Factors contributing to diurnal temperature range trends in twentieth and twenty-first century simulations of the CCCma coupled model, *Clim. Dynam.*, *20*, 435–445, doi: 10.1007/s00382-002-0288-y.

Trenberth, K. E., et al. (2007), Observations: Surface and Atmospheric Climate Change, in Climate Change 2007: The Physical Science Basis. Contribution of Working Group I to the Fourth Assessment Report of the Intergovernmental Panel on Climate Change, edited by Solomon, S., D. Qin, M. Manning, Z. Chen, M. Marquis, K. B. Averyt, M. Tignor and H. L. Miller, Cambridge University Press, Cambridge, United Kingdom and New York, NY, USA.

Vose, R. S., D. R. Easterling, and B. Gleason (2005), Maximum and minimum temperature trends for the globe: An update through 2004, *Geophys. Res. Lett.*, *32*(23), L23822, doi: 10.1029/2005GL024379.

Watterson, I. G. (1997), The diurnal cycle of surface air temperature in simulated present and doubled CO_2 climates, *Clim. Dynam.*, *13*, 533–545.

Walters, J. T., R. T. McNider, X. Shi, and W. B. Norris (2007), Positive surface temperature feedback in the stable nocturnal boundary layer, *Geophys. Res. Lett.*, *34*, L12709, doi:10.1029/2007/GL029505.

Wild, M., A. Ohmura, and K. Makowski (2007), Impact of global dimming and brightening on global warming, *Geophys. Res. Lett.*, *43*, L04702, doi:10.1029/2006GL028031.

Zhang, J., W.-C. Wang and L. Wu (2009), Land-atmosphere coupling and diurnal temperature range over the contiguous United States, *Geophys. Res. Lett.*, *36*, L06706, doi:10.1029/2009GL037505.

Zhang, J., L. Wu and W. Dong (2011), Land-atmosphere coupling and summer climate variability over East Asia, *J. Geophys. Res.*, *116*, D05117, doi:10.1029/2010JD014714.

Zhou, L., R. E. Dickinson, A. Dai, and P. Dirmeyer (2010), Detection and attribution of anthropogenic forcing to diurnal temperature range changes from 1950 to 1999: comparing multi-model simulations with observations, *Clim. Dynam.*, *35*(7–8), 1289–1307.